Computers and Mathematics with Applications 58 (2009) 1045–1054

Contents lists available at ScienceDirect

Computers and Mathematics with Applications

journal homepage: www.elsevier.com/locate/camwa

A comparison of non-Newtonian models for lattice Boltzmann blood flow simulations

Mahmud Ashrafizaadeh *, Hani Bakhshaei

Department of Mechanical Engineering, Isfahan University of Technology, Isfahan, 84156-83111, Iran

ARTICLE INFO

Keywords:
Lattice Boltzmann
Non-Newtonian fluid
Blood flow

ABSTRACT

In the present paper, three non-Newtonian models for blood are used in a lattice Boltzmann flow solver to simulate non-Newtonian blood flows. Exact analytical solutions for two of these models have been derived and presented for a fully developed 2D channel flow. Original results for the use of the K–L model in addition to the Casson and Carreau–Yasuda models are reported for non-Newtonian flow simulations using a lattice Boltzmann (LB) flow solver. Numerical simulations of non-Newtonian flow in a 2D channel show that these models predict different mass flux and velocity profiles even for the same channel geometry and flow boundary conditions. Which in turn, suggests a more careful model selection for more realistic blood flow simulations. The agreement between predicted velocity profiles and those of exact solutions is excellent, indicating the capability of the LB flow solver for such complex fluid flows.

1. Introduction

Metastases from a primary tumor to secondary locations throughout the body are a major cause of cancer related fatalities [1]. Since nothing can reach tumor cells without passing through blood flow, it seems reasonable to further investigate blood flow dynamics and its physical properties. Blood is a marvelous fluid that nurtures life, contains many enzymes and hormones and transports oxygen and carbon dioxide between the lungs and the cells of the tissues. It is a complex non-Newtonian fluid and its constitutive equation has an important role in hemodynamics and hemorheology. The study of most of these important functions of blood can be left to hematologists, biochemists, and pathological chemists. However, for biomechanics the most important information is the constitutive equation [1]. In this paper, we report original results of LB simulation of blood flows using three different non-Newtonian models, namely, the K–L model [2], the Casson model [3] and the Carreau–Yasuda model [4]. The LB model itself is a novel numerical approach that has recently been adapted to the field of blood rheology and particle interactions in blood flows. In this method, a discretized BGK form of the Boltzmann equation for the fluid particle distribution function is solved on a usually uniform Lattice. In the present work, an LB model for blood flow has been developed and for the first time, the K–L model in addition to the Cassons and Carreau Yasuda models have been implemented in an LB model. To validate the LB model, numerical results are compared with those of analytic solutions for a 2D blood flow between parallel plates where the governing equations can be solved analytically.

2. Lattice Boltzmann model

As a relatively new numerical scheme for simulating complex flow and transport phenomena, the LB model [5–8] provides an alternative approach particularly in cases where direct solution of the Navier–Stokes equations is not practical.

* Corresponding author.
E-mail address: mahmud@cc.iut.ac.ir (M. Ashrafizaadeh).

0898-1221/$ – see front matter © 2009 Elsevier Ltd. All rights reserved.
doi:10.1016/j.camwa.2009.02.021

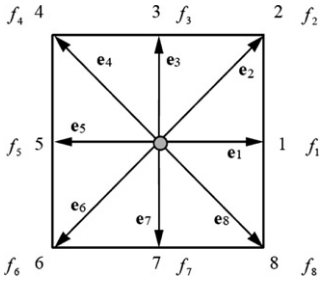

Fig. 1. D2Q9 lattice model.

Unlike conventional computational fluid dynamics methods which are based on macroscopic continuum equations, the LB model solves a mesoscopic LB equation to determine macroscopic fluid dynamics. The efficiency of this approach arises from its local nature where only the neighboring nodes need to be considered to update a particle distribution function, f, at each time step. Because of its flexibility and local nature, the code implementation and parallelization for an LB model is rather easier compared to that of a conventional computational fluid dynamics code. The LB model has been successfully applied to various physical problems, including single component hydrodynamics, multiphase and multicomponent fluid flows, magneto-hydrodynamics, reaction–diffusion systems, flows through porous media, and solid particle suspensions.

The LB model typically has an underlying Cartesian lattice in space as a consequence of the symmetry of the discrete particle velocity set and the fact that the lattice spacing δx is related to the time step size δt by $\delta x = c\delta t$, where c is the basic unit of the discrete lattice velocity set. This makes the LB model a simple scheme consisting of two essential steps: collision and streaming. The collision step models a simplified interaction among fluid particles and the streaming step simply moves particles from one lattice point to the other according to their velocity directions.

In an LB formulation, the single-particle distribution function, f, is discretized in time and space [9]. The LB model solves a discretized form of the Boltzmann equation for the fluid particle density distribution. We consider a 2D LB model with nine discrete velocities (the D2Q9 model) on a square lattice with uniform spacing. In the streaming step of the LB model, particles move from one node of the lattice to one of its neighbors as illustrated in Fig. 1. The discrete velocities are given by:

$$e_i = \begin{cases} (0,0) & i = 0 \\ \left(\cos\left[(i-1)\frac{\pi}{4}\right], \sin\left[(i-1)\frac{\pi}{4}\right]\right).c & i = 1,3,5,7 \\ \left(\cos\left[(i-1)\frac{\pi}{4}\right], \sin\left[(i-1)\frac{\pi}{4}\right]\right)\sqrt{2}.c & i = 2,4,6,8 \end{cases} \tag{1}$$

The discrete LB equation is:

$$f_i(x + e_i\delta t, t + \delta t) = f_i(x,t) + \Omega_i \tag{2}$$

where f_i is the particle distribution function in the i direction, Ω_i is a collision operator which could be given by the well-known BGK model [10,11] as follows:

$$\Omega_i = -\frac{1}{\tau}\left[f_i(x,t) - f_i^{eq}(x,t)\right] \tag{3}$$

where τ is a relaxation time and f_i^{eq} is the equilibrium distribution function which is determined by the local fluid density, ρ, and flow velocity, $\mathbf{u}$, as follows:

$$f_i^{eq} = \rho w_i\left[1 + \frac{3}{c^2}e_i\cdot\mathbf{u} + \frac{9}{2c^4}(e_i\cdot\mathbf{u})^2 - \frac{3}{2c^2}\mathbf{u}\cdot\mathbf{u}\right] \tag{4}$$

where w_i is a weighting factor given by:

$$w_i = \begin{cases} 4/9 & i = 0 \\ 1/9 & i = 1,3,5,7 \\ 1/36 & i = 2,4,6,8. \end{cases} \tag{5}$$

Once the particle distribution function is known, macroscopic properties such as density and momentum, can be obtained using the following relations:

$$\rho = \sum_{i=0}^{8} f_i = \sum_{i=0}^{8} f_i^{eq} \quad \text{and} \quad \rho u = \sum_{i=0}^{8} e_i f_i = \sum_{i=0}^{8} e_i f_i^{eq} \tag{6}$$

The speed of sound in this model is $c_s = c/\sqrt{3}$ and the equation of state is that of an ideal gas (i.e. $P = \rho c_s^2$). The kinematic viscosity is related to the time relaxation by $\nu = \frac{(2\tau-1)c^2\delta t}{6}$.

3. Non-Newtonian models

Based on the non-Newtonian fluid behaviour they are categorized into several groups, e.g. visco-elastic, visco-plastic, shear thinning and shear thickening fluids. Furthermore several constitutive equations have been proposed for the modelling of blood flow which are briefly discussed in this section.

3.1. Casson rheology model

This model can be described by the Casson equation [3]:

$$\sqrt{\sigma} = \sqrt{\eta_c}\sqrt{\dot{\gamma}} + \sqrt{\sigma_y} \quad \text{if } \sqrt{\sigma} > \sqrt{\sigma_y} \tag{7}$$

where σ is the shear stress, η_c is the Casson viscosity and σ_y is the yield stress. $\dot{\gamma}$ is the shear rate which is zero if $\sqrt{\sigma} \leq \sqrt{\sigma_y}$ in this model. For hematocrit[1] $H > 5.8$ the yield stress is found to be given by:

$$\sigma_y^{1/3} = \frac{A(H - H_c)}{100} \tag{8}$$

where $A = (0.008 \pm 0.002)^{1/3}\text{dyne/cm}^2$, H is the normal hematocrit and H_c is the critical hematocrit below which there is no yield stress [3].

3.2. Carreau–Yasuda model

In order to account for the shear thinning property of blood flow, Carreau–Yasuda model suggests the following equation [4] which incorporates two limiting viscosities μ_0 and μ_∞:

$$\frac{\mu - \mu_\infty}{\mu_0 - \mu_\infty} = \left[1 + (\lambda\dot{\gamma})^a\right]^{\frac{n-1}{a}} \tag{9}$$

where $n < 1$ and λ are two curve fitting parameters and a is a model constant (in the present work $a = 0.644$, $n = 0.392$, $\lambda = 0.11$, $\mu_0 = 22 \times 10^{-3}$ and $\mu_\infty = 2.2 \times 10^{-3}$ [12]). This model can describe shear thinning behaviour over wide ranges of shear rates but only at the expense of the added complexity of some extra parameters. This model predicts Newtonian fluid behaviour $\mu = \mu_0$ when either $n = 1$ or $\lambda = 0$ or both.

3.3. K–L model

Experiments have shown that the behaviour of blood, a suspension of cells in plasma, can be modelled with a pseudoplastic and a following Newtonian region in a shear stress versus shear rate scale. According to this model, the following constitutive equation for blood is suggested in the K–L model [2]:

$$\begin{aligned} &\sigma = \sigma_y + \eta_2\dot{\gamma}^{1/2} + \eta_1\dot{\gamma} \quad \dot{\gamma} \leq \dot{\gamma}_c\ \sigma > \sigma_y \\ &\dot{\gamma} = 0 \quad \sigma \leq \sigma_y \end{aligned} \tag{10}$$

where the three parameters σ_y, η_1 and η_2 are functions of hematocrit, plasma viscosity and other variables. γ_c is the critical shear rate beyond which the flow becomes turbulent [2]. The first two terms of Eq. (10) are responsible for the shear thinning effect of blood and the third term is the Newtonian contribution. Clearly the K–L model is an improved modification of the Casson model and is more general. If $\eta_2 = 2\sqrt{\eta_1\sigma_y}$ is substituted in Eq. (10), the K–L model becomes the Casson equation, as follows:

$$\sigma = \sigma_y + 2\sqrt{\eta_1\sigma_y}\dot{\gamma}^{1/2} + \eta_1\dot{\gamma} = \left(\sqrt{\sigma_y} + \sqrt{\eta_1\dot{\gamma}}\right)^2 \tag{11}$$

which is the same as Eq. (7) provided that η_1 is set equal to η_c. In addition, if the yield stress is zero ($\sigma_y = 0$), then the Casson equation simply describes Newtonian fluids, while the K–L model is still of shear thinning property.

4. Lattice Boltzmann and non-Newtonian flows

Early extension of the LB model to simulate non-Newtonian fluid flows has been reported by Aharonov and Rothman [13]. Gabbanelli, Drazer and Koplic [14] have extensively tested the accuracy of the LB model for non-Newtonian fluid flows using the truncated power-law model. Kehrwald [15] simulated a shear thinning flow using the Carreau–Yasuda model and instead of using velocity gradients, used intrinsic quantities of the LB model to calculate the strain rate. A second order accurate LB model was developed by Boyd, Buick and Green [16] to study shear thinning and shear thickening flow behaviour for a range of power-law model parameters. The same authors have analysed steady and unsteady flows using the LB model with Casson and Carreau–Yasuda non-Newtonian models and reported significant differences between those results [17]. The Casson model has also been used by Ouared and Chopard [18] for non-Newtonian fluid flow simulations. Boyd and

[1] The hematocrit is the proportion, by volume, of the blood that consists of red blood cells.

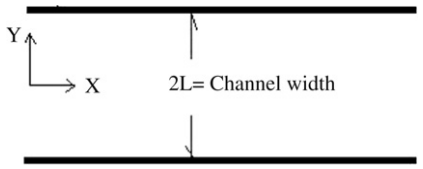

Fig. 2. 2D channel geometry.

Buick [19] has compared the Newtonian and non-Newtonian (i.e. Carreau–Yasuda) models for blood flow in a realistic 2D carotid artery geometry and reported a generally small difference between the results, suggesting a safe neglect of the non-Newtonian nature of blood under certain conditions. The Carreau–Yasuda model has also been used by Bernsdorf and Wang [20] and Malaspinas, Courbebaisse and Deville [21] to simulate blood flow in cerebral aneurysms and flow through a 4–1 planar contraction, respectively.

Essentially, an LB simulation of non-Newtonian fluid consists of determining the value of the relaxation time locally in such a way that the desired local value of the viscosity is recovered. One should note that the viscosity itself is related to the local rate of strain through the constitutive equation for the stress tensor as given for different non-Newtonian models [13,14,18].

In this paper, three non-Newtonian models for blood have been implemented in an LB flow solver. In particular, the applicability of the K–L model is compared with that of the Casson model for the blood flow simulation. The K–L model is a rather new multiparameter equation for blood where as the Casson model is considered as one of the most popular models in this field. To the best of authors' knowledge, the more recent K–L model for non-Newtonian flow has not been incorporated in an LB model. To implement a non-Newtonian model in the LB model, after obtaining the instantaneous velocity field, the strain rate tensor, S_{ij}, is computed using a first order finite difference approximation of the local derivatives of the velocity field. The magnitude of the local shear rate, $\dot{\gamma}$, is related to the second invariant of the strain rate tensor (i.e. $\dot{\gamma} = \sqrt{S_{ij}S_{ij}}$), where the components of the strain rate tensor are computed locally from the velocity field. After calculation of $\dot{\gamma}$, fluid viscosity must be computed. Following the general definition of the apparent viscosity ($\sigma = \mu(\dot{\gamma})\dot{\gamma}$) and using Eq. (10) for the K–L model one obtains the following expression for μ as a function of the shear strain rate:

$$\mu = \frac{\sigma_y + \eta_2 \dot{\gamma}^{1/2} + \eta_1 \dot{\gamma}}{\dot{\gamma}}. \tag{12}$$

In order to calculate the local relaxation time, the following equation is used:

$$\tau = \left(\frac{3}{c^2 \rho \delta t}\mu + \frac{1}{2}\right). \tag{13}$$

This relaxation time is renewed in each time step and is used in the LB equation for the next time step. Other non-Newtonian models are implemented in the LB flow solver in a similar manner.

5. Problem definition and analytical velocity profiles

As a benchmark, a 2D flow through a straight channel has been considered for which exact solutions of the K–L and the Casson models can be derived to validate the present numerical results. In Fig. 2 the channel geometry is shown.

For the case of fluid flow between two parallel plates, the application of conservation of momentum leads to the following equation:

$$\sigma = \mu \frac{\partial U}{\partial y} = y \frac{\partial P}{\partial x} \tag{14}$$

where U is the flow velocity in axial, x, direction and P is the pressure. This equation is valid for both Newtonian and non-Newtonian laminar, steady-state fully developed flows. Using Eq. (14), y_c, the position where the shear stress is equal to the yield stress is obtained as follows:

$$y_c = \sigma_y \left(\frac{\partial P}{\partial x}\right)^{-1} \tag{15}$$

and from the Casson model rheology, one obtains:

$$\dot{\gamma} = \frac{1}{\eta_c}(\sigma + \sigma_y - 2\sqrt{\sigma \sigma_y}). \tag{16}$$

By substituting Eqs. (14) and (15) into Eq. (16), the exact velocity profile for the Casson model can be obtained (see [22] for details):

$$U(y) = \frac{1}{\eta_c}\frac{\partial P}{\partial x}\left(\frac{y^2 - L^2}{2} + y_c(|y| - L) - \frac{4}{3}\sqrt{y_c}(\sqrt{|y|^3} - \sqrt{L^3})\right). \tag{17}$$

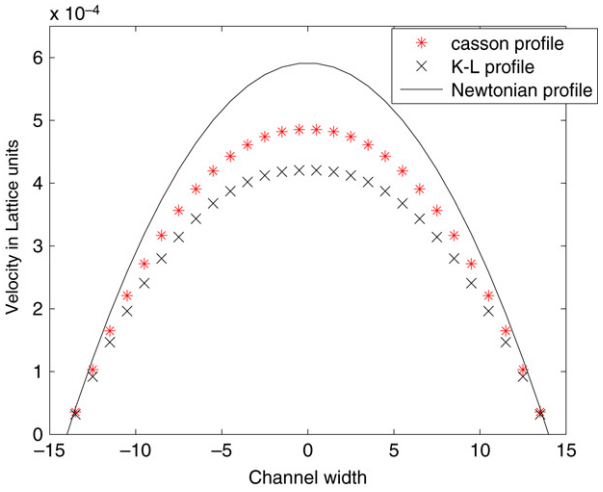

Fig. 3. Exact velocity profiles for flow in a 2D channel.

For $y < y_c$ the shear rate is zero. Therefore, the velocity will not change and as a result, in this region, we have:

$$U(y) = U(y_c) \quad y < y_c. \tag{18}$$

In order to calculate the analytic velocity profile for the K–L model, a similar procedure is followed, but some differences should be considered. The shear rate, $\dot{\gamma}$, is obtained from Eq. (10) and by introducing σ_α such that:

$$\sigma_\alpha = \frac{\eta_2^2}{4\eta_1} - \sigma_y \tag{19}$$

from Eq. (15) we have:

$$y_\alpha = \sigma_\alpha \left(\frac{\partial P}{\partial x}\right)^{-1} \tag{20}$$

where y_α is the position at which $\sigma = \sigma_\alpha$. In Eq. (19) $\sigma_\alpha + \sigma_y$ is the stress caused purely by shear thinning effect of blood. therefore, σ_α could be considered as a measure of the difference between the K–L and the Casson models. Solving Eq. (10) leads to:

$$\begin{aligned} \dot{\gamma} &= \frac{2\eta_2^2 - 4\eta_1\left(\sigma_y + \frac{\partial P}{\partial x} y\right) - 2\eta_2\sqrt{\Delta}}{4\eta_1^2} \\ \Delta &= \eta_2^2 - 4\eta_1\left(\sigma_y + \frac{\partial P}{\partial x} y\right). \end{aligned} \tag{21}$$

Following the above equation and after some algebra [22], the analytical solution of the K–L model is obtained:

$$U(y) = -\frac{1}{4\eta_1}\frac{\partial P}{\partial x}\left[2(L^2 - y^2) + (8y_\alpha + 4y_c)(L - |y|) - \frac{16}{3}\sqrt{y_c + y_\alpha}\left(\sqrt{L + y_\alpha} - \sqrt{|y| + y_\alpha}\right)\right]. \tag{22}$$

One should note that if $\sigma_\alpha = y_\alpha = 0$ then Eq. (22) resembles the Casson profile given by Eq. (17). On the other hand, if $\sigma_\alpha = \sigma_y = 0$ that is $y_\alpha = y_c = 0$, then the above equation simply describes a Newtonian flow. However, if only the yield stress is zero, $\sigma_y = 0$, then the Casson equation simply describes a Newtonian fluid, where as the K–L model still presents some shear thinning property.

Fig. 3 shows the analytical velocity profiles for flow through a 2D channel using the Newtonian as well as the Casson and K–L non-Newtonian models. The flow in this channel for all three models is driven under the influence of a same pressure gradient, $\frac{\partial P}{\partial x}$. For the Newtonian model, it can be shown that the Reynolds number, *Re*, is:

$$Re = \frac{\rho \frac{\partial P}{\partial x}(2L)^3}{12\mu^2}. \tag{23}$$

The presented profiles in Fig. 3 are for flows at $Re = 400$ assuming $\eta_1 = 4.076$ mpas, $\eta_2 = 16.06$ mpas$^{1/2}$, and $\sigma_y = 4.968$ mpa for the K–L model. The Newtonian viscosity and η_c in the Casson model are assumed to be equal to η_1.

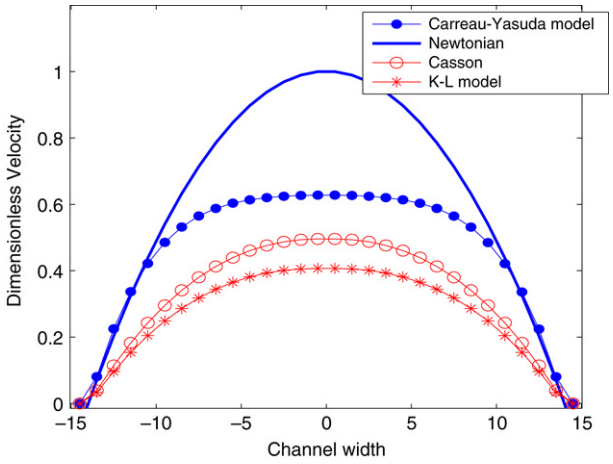

Fig. 4. Exact dimensionless velocity profiles for flow in a 2D channel for different models.

6. Numerical model

To implement the LB model, a D2Q9 lattice is used. All variables in the LB model are defined in lattice units, which should be properly converted to physical units when real values are needed. To start the computations, a uniform field is used to initialize velocity and density fields. A mid-grid bounce back boundary condition [6] is used for solid walls and the periodic boundary condition is set at both inlet and outlet boundaries. For each flow simulation, a prescribed pressure gradient based on the desired *Re* number (Eq. (23)), is used as a body force in the LB model.

For Newtonian fluids, relaxation time and viscosity are constant. However, for non-Newtonian fluids, viscosity is a function of the velocity gradient, as discussed before. This causes a relaxation time variation across the channel in the LB model. Due to the initial uniform flow field, the velocity gradients are zero at the initial time steps. In addition, the velocity gradient vanishes in certain regions of the flow field (e.g. along the channel centerline). As a consequence, the calculated viscosity goes to infinity. In order to continue with the numerical solution and prevent a division by zero, a small value equal to the machine epsilon is added to the velocity gradient when it becomes zero.

7. Results and discussions

In this section, numerical results are presented and compared against exact solutions where possible. Both numerical and exact values are normalized by the centerline velocity of a Newtonian flow under the same physical condition (i.e. the same *Re* number and pressure gradient). Fig. 4 shows the numerical non-dimensional velocity profiles for the three non-Newtonian models. The flow for all three simulations is driven by the same pressure gradient. The corresponding defined Reynolds number is 270. As is shown in Fig. 4, the three models predict different velocity profiles for the non-Newtonian flow even under the same physical situation. The Carreau–Yausuda model predicts the maximum flow rate through the channel and a flatter velocity profile. On the other hand, the K–L model gives the lowest flow rate and a velocity profile with less flatness at the center of the channel. These different results suggest a more careful non-Newtonian model selection for real blood flow simulations.

The development of the velocity profile at different flow *Re* number for the K–L model is shown in Fig. 5. As the *Re* number increases, the velocity profile approaches a more parabolic shape and approaches a Newtonian-like profile. One should note that the dimensionless velocity profiles for a Newtonian flow at different *Re* numbers are identical. These numerical results are confirmed by experimental observation which states that blood is almost Newtonian at higher shear rates, while at low shear rates exhibits yield stress and non-Newtonian behaviour [3].

In order to validate the present LB results, theoretical and numerical velocity profiles at different *Re* numbers for the K–L and the Casson models are shown in Figs. 6 and 7, respectively.

To obtain these steady-state results using the LB flow solver, a time trace of the centerline velocity is monitored during the simulations. As an example, a centerline velocity development is shown in Fig. 8 for a flow at $Re = 100$ using the Casson model.

In addition, to terminate the numerical simulations, a convergence criterion, as defined below, is used.

$$\epsilon = \frac{1}{LY} \sum_{i=1}^{LY} \frac{\|U(y_i, t) - U(y_i, t-1)\|}{U(y_i, t)} \tag{24}$$

where LY is the number of lattice nodes across the channel and U is the axial flow velocity component at different y_i locations across the channel at times t and $t-1$. A value of at least 10^{-10} is used to terminate the numerical simulations for the results

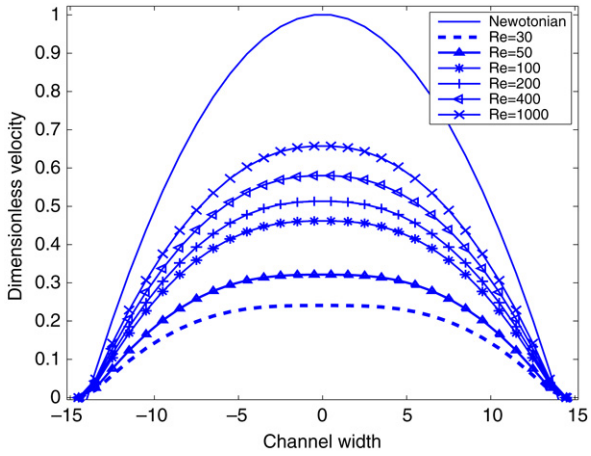

Fig. 5. Exact dimensionless velocity profiles for flow in a 2D channel for the K–L model.

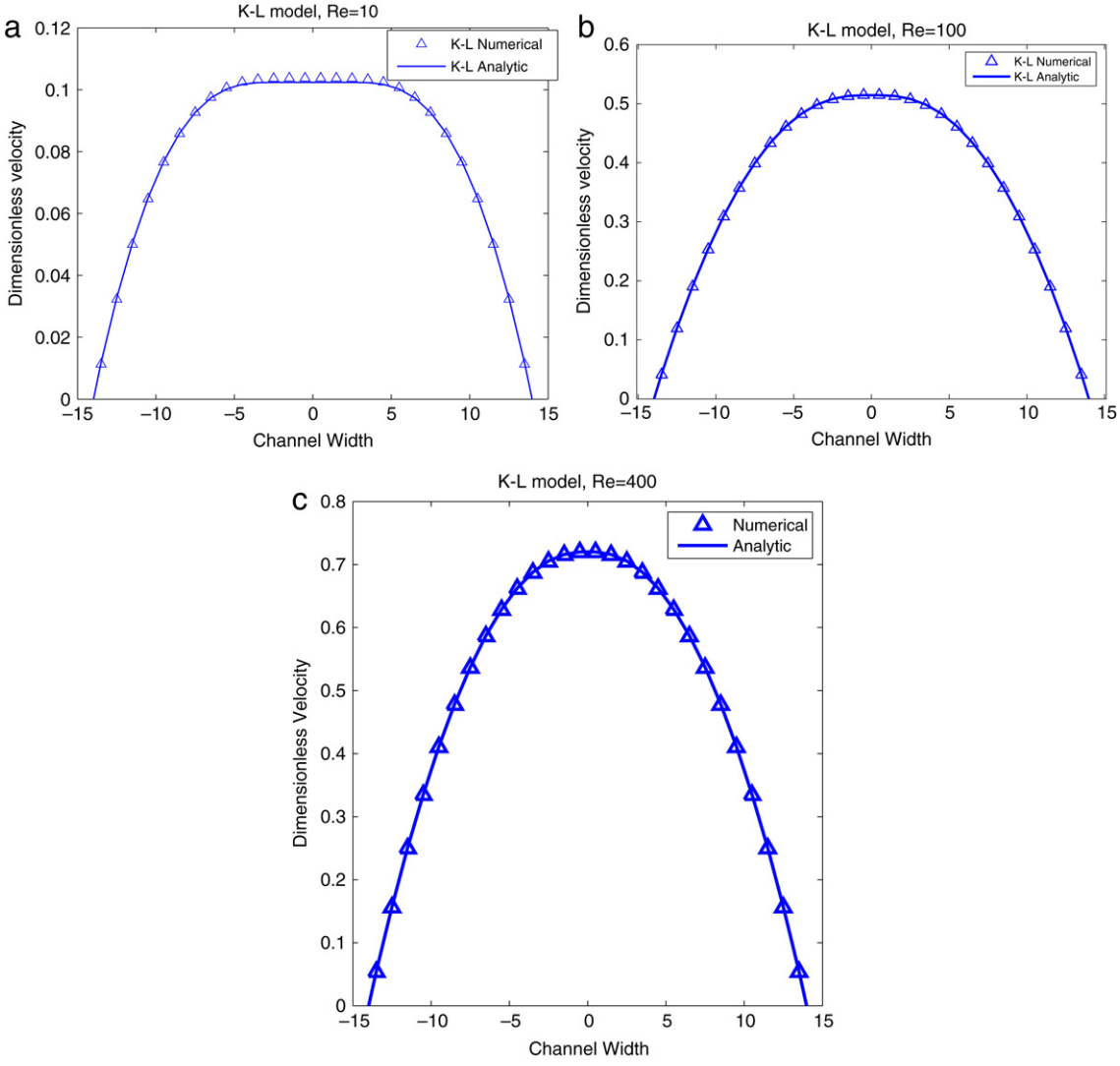

Fig. 6. A comparison between numerical and exact velocity profiles for the K–L model.

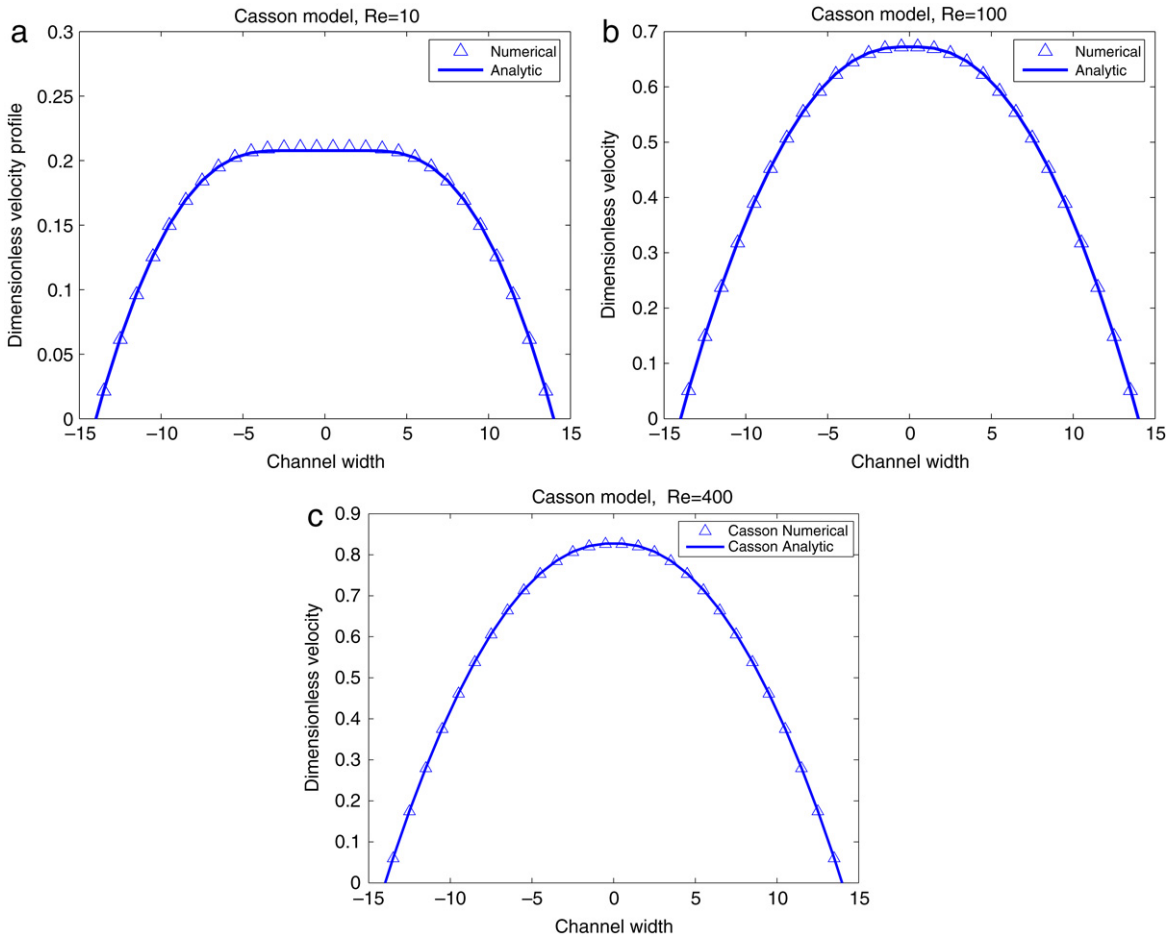

Fig. 7. A comparison between numerical and exact velocity profiles for the Casson model.

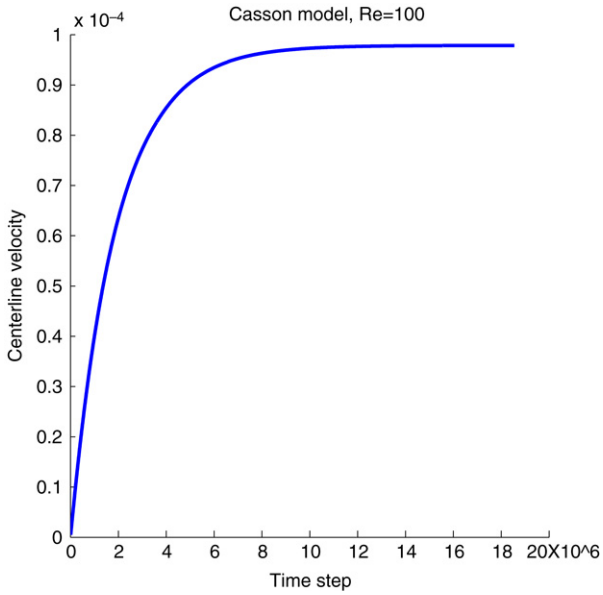

Fig. 8. Time development of centerline velocity.

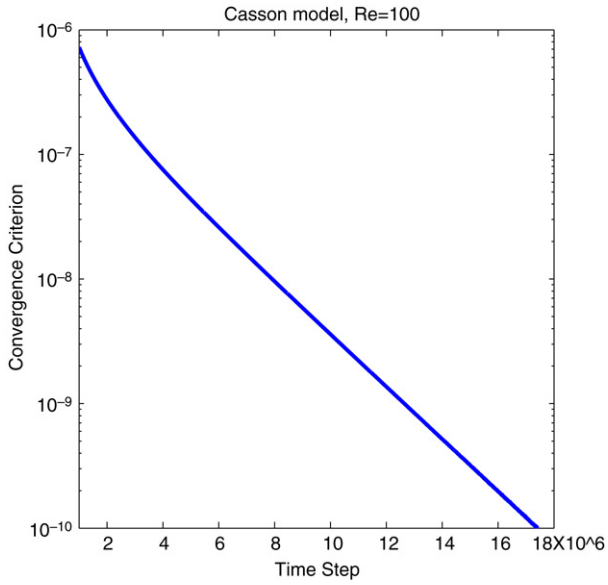

Fig. 9. Variation of convergence criterion with time.

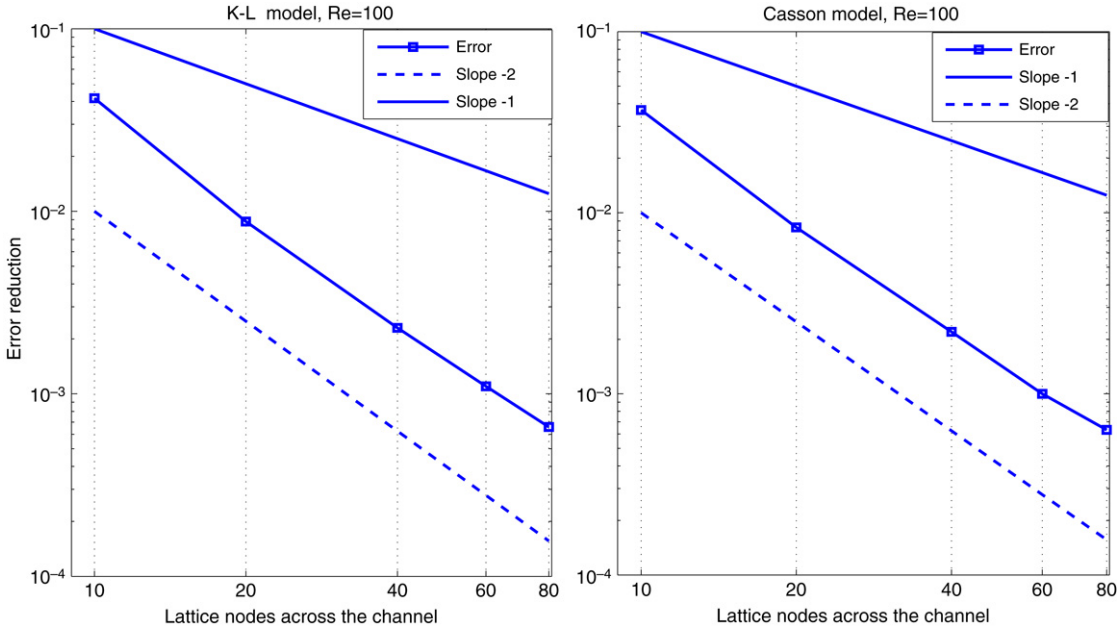

Fig. 10. Effect of the lattice size on numerical error.

presented. A typical convergence rate reduction is shown in Fig. 9 for a flow at $Re = 100$ using the Casson model. As is shown, the convergence criterion is steadily decreasing.

In order to investigate the effect of the lattice size on the numerical accuracy and quantify the numerical error, a series of flow simulations are conducted using different lattice sizes. Fig. 10 shows the error reduction versus the number of lattice nodes across the channel for both K–L and the Casson models. The error is defined here by:

$$error = \frac{1}{LY}\sum_{i=1}^{LY}\frac{\|U(y_i)_{exact} - U(y_i)_{numeric}\|}{U(y_i)_{exact}}. \tag{25}$$

In these simulations, the number of lattice nodes across the channel is increased from 10 to 80. As is shown in Fig. 10 a second order error reduction, consistent with reported results by others [5,16], is obtained and the numerical error is quite low.

Table 1
Number of time steps for different flow simulations.

Re	10	100	400
Casson model	10.31×10^6	17.43×10^6	19.07×10^6
K–L model	6.17×10^6	15.02×10^6	17.8×10^6

It is observed that the number of time steps to reach a steady-state solution increases with the flow *Re* number. Table 1 presents the number of time steps required to satisfy the abovementioned convergence criterion for non-Newtonian flows at different *Re* numbers and using different models.

8. Summary and conclusions

A D2Q9 LB model has been developed to simulate non-Newtonian fluid flows. For the first time the K–L model in addition to the Casson and Carreau–Yasuda models has been incorporated in a lattice Boltzmann model. Predicted velocity profiles by the non-Newtonian LB model for a channel flow have an excellent agreement with those of exact solutions, presenting the capability of the LB model for the non-Newtonian fluid flow simulation. Different results obtained from different non-Newtonian models suggest a more careful model selection for real blood flow simulations.

References

[1] Y.C. Fung, Biomechanics, Mechanical Properties of Living Tissues, 2nd ed., Springer, New York, 1993.
[2] X.Y. Luo, Z.B. Kuang, A study on the constitutive equation of blood, Journal of Biomechanics 25 (1992) 929.
[3] J.N. Mazumdar, Biofluid Mechanics, World Scientific, Singapore, 1992.
[4] R.B. Bird, R.C. Armstrong, O. Hassager, Dynamics of Polymer Liquids. Vol. I. Fluid Mechanics, 2nd ed., Wiley, New York, 1987.
[5] S. Chen, G.D. Doolen, Lattice Boltzmann method for fluid flows, Annual Review of Fluid Mechanics 30 (1998) 329.
[6] S. Succi, The Lattice Boltzmann Method for Fluid Dynamics and Beyond, Clarendon Press, Oxford, UK, 2001.
[7] D.A. Wolf-Gladrow, Lattice-Gas Cellular Automata and Lattice Boltzmann Models, Springer, New York, 2000.
[8] X. He, L.-S. Luo, Lattice Boltzmann model for the incompressible Navier–Stokes equation, Journal of Statistical Physics 88 (1997) 927.
[9] C. Sun, L.L. Munn, Particulate nature of blood determines macroscopic rheology: A 2-D lattice Boltzmann analysis, Biophysical Journal 88 (2005) 1635.
[10] P. Bhatnagar, E.P. Gross, M.K. Krook, A model for collision processes in gases. I. Small amplitude processes in charged and neural one-component systems, Physical Review 94 (3) (1954) 511.
[11] Y.H. Qian, D. d'humières, P. Lallemand, Lattice BGK models for the Navier–Stokes equation, Europhysics Letters 17 (1992) 479.
[12] F.J.H. Gijsen, F.N. van de Vosse, J.D. Janssen, The influence of the non-Newtonian properties of blood on the flow in large arteries: Steady flow in carotid bifurcation model, Journal of Biomechanics 32 (1999) 601.
[13] E. Aharonov, D.H. Rothman, Non-Newtonian flow (through porous-media): A lattice Boltzmann method, Geophysical Research Letters 20 (8) (1993) 679.
[14] S. Gabbanelli, G. Drazer, J. Koplik, Lattice Boltzmann method for non-Newtonian (power-law) fluids, Physical Review E 72 (4) (2005) 046312.
[15] D. Kehrwald, Lattice Boltzmann simulation of shear thinning fluids, Journal of Statistical Physics 121 (2005) 223.
[16] J. Boyd, J. Buick, S. Green, A second-order accurate lattice Boltzmann non-Newtonian flow model, Journal of Physics A 39 (46) (2006) 14241.
[17] J. Boyd, J.M. Buick, S. Green, Analysis of the Casson and Carreau–Yasuda non-Newtonian blood models in steady and oscillatory flows using the lattice Boltzmann method, Physics of Fluids 19 (9) (2007) 093103.
[18] R. Ouared, B. Chopard, Lattice Boltzmann simulation of blood flow: Non-Newtonian rheology and clotting processes, Journal of Statistical Physics 121 (2005) 209.
[19] J. Boyd, J.M. Buick, Comparison of Newtonian and non-Newtonian flows in a two-dimensional carotid artery model using the lattice Boltzmann model, Physics in Medicine and Biology 52 (20) (2007) 6215.
[20] J. Bernsdorf, D. Wang, Non-Newtonian blood flow simulation in cerebral aneurysms, Computer & Mathematics with Applications 58 (5) (2009) 1024.
[21] O. Malaspinas, G. Courbebaisse, M. Deville, Simulation of generalized Newtonian fluids with the lattice Boltzmann Method, International Journal of Modern Physics C 18 (12) (2007) 1939.
[22] H. Bakhshaei, Lattice Boltzmann simulation of Non-Newtonian fluid flows, M.Sc. Thesis, Dept. of Mech. Eng., Isfahan Univ. of Tech., Isfahan, Iran, 2008.